Astronomy & Astrophysics

Turbulent viscosity and magnetic Prandtl number from simulations of isotropically forced turbulence

P. J. Käpylä[1,2], M. Rheinhardt[2], A. Brandenburg[3,4,5,6], and M. J. Käpylä[7,2]

[1] Georg-August-Universität Göttingen, Institut für Astrophysik, Friedrich-Hund-Platz 1, 37077 Göttingen, Germany
e-mail: pkaepyl@uni-goettingen.de
[2] ReSoLVE Centre of Excellence, Department of Computer Science, Aalto University, PO Box 15400, 00076 Aalto, Finland
[3] Nordita, KTH Royal Institute of Technology and Stockholm University, Roslagstullsbacken 23, 10691 Stockholm, Sweden
[4] Department of Astronomy, Stockholm University, 10691 Stockholm, Sweden
[5] JILA and Department of Astrophysical and Planetary Sciences, Box 440, University of Colorado, Boulder, CO 80303, USA
[6] Laboratory for Atmospheric and Space Physics, 3665 Discovery Drive, Boulder, CO 80303, USA
[7] Max-Planck-Institut für Sonnensystemforschung, Justus-von-Liebig-Weg 3, 37077 Göttingen, Germany

ABSTRACT

Context. Turbulent diffusion of large-scale flows and magnetic fields plays a major role in many astrophysical systems, such as stellar convection zones and accretion discs.
Aims. Our goal is to compute turbulent viscosity and magnetic diffusivity which are relevant for diffusing large-scale flows and magnetic fields, respectively. We also aim to compute their ratio, which is the turbulent magnetic Prandtl number, $\mathrm{Pm_t}$, for isotropically forced homogeneous turbulence.
Methods. We used simulations of forced turbulence in fully periodic cubes composed of isothermal gas with an imposed large-scale sinusoidal shear flow. Turbulent viscosity was computed either from the resulting Reynolds stress or from the decay rate of the large-scale flow. Turbulent magnetic diffusivity was computed using the test-field method for a microphysical magnetic Prandtl number of unity. The scale dependence of the coefficients was studied by varying the wavenumber of the imposed sinusoidal shear and test fields.
Results. We find that turbulent viscosity and magnetic diffusivity are in general of the same order of magnitude. Furthermore, the turbulent viscosity depends on the fluid Reynolds number (Re) and scale separation ratio of turbulence. The scale dependence of the turbulent viscosity is found to be well approximated by a Lorentzian. These results are similar to those obtained earlier for the turbulent magnetic diffusivity. The results for the turbulent transport coefficients appear to converge at sufficiently high values of Re and the scale separation ratio. However, a weak trend is found even at the largest values of Re, suggesting that the turbulence is not in the fully developed regime. The turbulent magnetic Prandtl number converges to a value that is slightly below unity for large Re. For small Re we find values between 0.5 and 0.6 but the data are insufficient to draw conclusions regarding asymptotics. We demonstrate that our results are independent of the correlation time of the forcing function.
Conclusions. The turbulent magnetic diffusivity is, in general, consistently higher than the turbulent viscosity, which is in qualitative agreement with analytic theories. However, the actual value of $\mathrm{Pm_t}$ found from the simulations ($\approx 0.9-0.95$) at large Re and large scale separation ratio is higher than any of the analytic predictions ($0.4-0.8$).

Key words. turbulence – Sun: rotation – stars: rotation

1. Introduction

Turbulent transport is often invoked to explain phenomena in astrophysical systems such as accretion (e.g. Shakura & Sunyaev 1973; Frank et al. 2002), maintenance of stellar differential rotation (Rüdiger 1980, 1989; Rüdiger et al. 2013), and large-scale magnetic field generation (Moffatt 1978; Krause & Rädler 1980). Turbulence is typically thought to diffuse large-scale structures analogously to molecular diffusion but at a rate that is several orders of magnitude higher (e.g. Väisälä et al. 2014).

Turbulent diffusion coefficients, such as turbulent viscosity (ν_t) and magnetic diffusivity (η_t), are often estimated using arguments from the mixing length theory (MLT) according to which $\nu_t \approx \eta_t \approx ul/3$, where u and l are the characteristic velocity and length scale of the turbulence. Such estimates yield values of the order of $10^8-10^9 \, \mathrm{m^2 \, s^{-1}}$ for the solar convection zone, which coincide with values estimated for the turbulent magnetic diffusivity η_t from sunspot decay in the quenched case

(Krause & Rüdiger 1975; Petrovay & van Driel-Gesztelyi 1997; Rüdiger & Kitchatinov 2000) and from cross helicity measurements in the unquenched (quiet Sun) case (Rüdiger et al. 2011). With the advent of the test-field method (Schrinner et al. 2005, 2007), it has become possible to measure turbulent transport coefficients that are relevant for the electromotive force (e.g., the turbulent magnetic diffusivity) from simulations. Detailed studies using this method indicate that the MLT estimate yields the correct order of magnitude in the kinematic regime (e.g. Sur et al. 2008; Käpylä et al. 2009a), provided that l is identified with the inverse of the wavenumber k_f of the energy-carrying eddies. This result can further be affected by other physical properties, such as the presence of kinetic helicity in the flow, which can reduce the value of η_t (Brandenburg et al. 2017). The test-field method also revealed an approximately Lorentzian dependence on the wavenumber of the mean field (Brandenburg et al. 2008a).

In the absence of a corresponding test-field method for hydrodynamics, the estimates of ν_t are typically much less

accurate than those obtained for η_t from such methods. Estimates of turbulent viscosity from shearing box simulations, however, also indicate a value of the order of the MLT estimate (e.g. Snellman et al. 2009; Käpylä et al. 2010). Computing ν_t from simulations with imposed linear shear flows is problematic due to hydrodynamical instabilities that can be excited (e.g. Elperin et al. 2003; Käpylä et al. 2009b). Furthermore, also non-diffusive contributions to the turbulent stress exist. First, the anisotropic kinetic alpha (AKA) effect can occur in the presence of Galilean non-invariant flows[1] and can give rise to hydrodynamic instabilities analogous to the electromagnetic dynamo (e.g. Frisch et al. 1987; Brandenburg & von Rekowski 2001; Käpylä et al. 2018)[2]. Second, anisotropic turbulence with global rotation leads to a Λ effect, which is relevant for causing differential rotation (e.g. Rüdiger 1989; Kitchatinov & Rüdiger 2005; Käpylä & Brandenburg 2008; Käpylä 2019a). Typically, these effects cannot easily be disentangled from the contribution of turbulent viscosity. Additionally, a spatially non-uniform kinetic helicity Yokoi & Brandenburg (2016) in rotating non-mirror symmetric flows leads to the generation of large-scale flows.

Contrary to the microphysical magnetic Prandtl number, which can vary over tens of orders of magnitude in the astrophysical context, depending on the physical characteristics of the system under study (e.g. Brandenburg & Subramanian 2005), the ratio of ν_t to η_t, that is the turbulent magnetic Prandtl number Pm_t, is thought to be of the order of unity in the astrophysically relevant regime of high Reynolds numbers. Nevertheless, astrophysical applications of the possibility of Pm_t being different from unity have been discussed. These include both accretion disc turbulence and solar convection. In the context of accretion onto a magnetised star, one often assumes that the field lines of the star's magnetic field are being dragged with the flow towards the star, so as to achieve a pitch angle suitable for jet launching (Blandford & Payne 1982). This requires the turbulent magnetic diffusivity to be small (Elstner & Rüdiger 2000), while subsequent work has shown that Pm_t has only a weak influence on the pitch angle (Rüdiger & Shalybkov 2002).

Another application has been suggested in the context of the solar convection zone. For flux transport dynamos to explain the equatorward migration of the sunspot belts, one must assume the turbulent magnetic diffusivity to be of the order of $10^7 \, \text{m}^2 \, \text{s}^{-1}$ (Chatterjee et al. 2004). On the other hand, to prevent the contours of constant angular velocity from being constant on cylinders, the turbulent viscosity must be around $10^9 \, \text{m}^2 \, \text{s}^{-1}$, or even larger (Brandenburg et al. 1990). Thus, again, a turbulent magnetic Prandtl number in excess of unity is required for this model to be successful. A large turbulent viscosity is sometimes argued to be a consequence of the magnetic stress from small-scale dynamo action (Karak et al. 2018). Whether this idea has a solid foundation remains open, however.

The analytic estimates of the turbulent magnetic Prandtl number range between 0.4 under the first-order smoothing approximation (FOSA) to 0.8 under various versions of the τ approximation (Yousef et al. 2003; Kitchatinov et al. 1994), of which the spectral minimal τ approximation (MTA) applied to fully developed turbulent convection yields values in the range 0.23−0.46 (Rogachevskii & Kleeorin 2006). Different renormalisation group analyses yield $Pm_t \approx 0.42$−0.79 (e.g.

Fournier et al. 1982; Kleeorin & Rogachevskii 1994; Verma 2001; Jurčišinová et al. 2011). Furthermore, the turbulent magnetic Prandtl number has been studied from simulations of forced turbulence with a decaying large-scale field component by Yousef et al. (2003) who found that Pm_t is approximately unity irrespective of the microphysical magnetic Prandtl and Reynolds numbers. However, their dataset is limited to a few representative cases that do not probe the Reynolds number or scale dependences systematically.

Our aim is to compute the turbulent viscosity and turbulent magnetic Prandtl number from direct simulations of homogeneous isotropically forced turbulence where we systematically vary the Reynolds number and scale separation ratio and compare the obtained results with analytic ones. To achieve this, we impose a large-scale shear flow with a harmonic profile on the (non-rotating) flow and determine the turbulent viscosity either from the generated Reynolds stresses or from the decay rate of the large-scale flow. For obtaining the turbulent magnetic diffusivity we employ the test-field method.

2. Model

2.1. Basic equations

We model a compressible gas in a triply periodic cube with edge length L. It obeys an isothermal equation of state defined by $p = c_s^2 \rho$, with pressure p, density ρ and constant speed of sound c_s. Hence, we solve the continuity and Navier–Stokes equations with both an imposed random and large-scale shear forcing

$$\frac{D \ln \rho}{Dt} = -\nabla \cdot U, \tag{1}$$

$$\frac{DU}{Dt} = -c_s^2 \nabla \ln \rho + \frac{1}{\rho} \nabla \cdot (2\nu\rho \mathsf{S}) + f - \frac{1}{\tau}\left(\overline{U}_y - \overline{U}_y^{(0)}\right)\hat{e}_y, \tag{2}$$

where $D/Dt = \partial/\partial t + U \cdot \nabla$ is the advective time derivative, U is the velocity, ν is the constant kinematic viscosity, $\mathsf{S}_{ij} = \frac{1}{2}(U_{i,j} + U_{j,i}) - \frac{1}{3}\delta_{ij}\nabla \cdot U$ is the traceless rate of strain tensor, and the commas denote spatial derivatives. The forcing function f is given by

$$f = f_0 N(t) f_k(t) \,\text{Re}\left\{\exp\left[i(k(t) \cdot x + \phi(t))\right]\right\}, \tag{3}$$

where $k(t)$ is a random wavevector and

$$f_k(t) = (k \times e(t))/\sqrt{k^2 - (k \cdot e(t))^2} \tag{4}$$

is used to produce a nonhelical transversal sinusoidal f, where $e(t)$ is an arbitrary random unit vector, not aligned with k, and $\phi(t)$ is a random phase. $N(t) = c_s^{3/2}(k/\delta t)^{1/2}$ is a normalisation factor, $k = |k|$, δt is the length of the integration time step and f_0 is a constant dimensionless scaling factor. The quantities k, e, and ϕ change at every time step, so that the external force is delta-correlated (white) in time. Numerically, we integrate the forcing term by using the Euler–Maruyama scheme (Higham 2001). We consider models where k is within a narrow shell of wavevectors with k close to a chosen k_f, and determined such that the forcing always obeys the periodic boundary conditions.

The last term in Eq. (2) maintains a large-scale shear flow on top of the forced background turbulence via relaxing the horizontally (xy) averaged part of the y velocity, indicated by the overbar, towards the temporally constant profile $\overline{U}_y^{(0)}$; $\hat{e}_y$ is the unit vector in the y-direction. The relaxation time scale τ is chosen to match the turnover time $(u_{\text{rms}}k_f)^{-1}$ of the turbulence, where u_{rms} is the rms value of the fluctuating velocity,

---

[1] More precisely one had to speak about flows whose statistical properties are Galilean invariant or non-invariant.

[2] In those papers, the presence of a deterministic forcing function made the flow Galilean non-invariant.

$u_{\mathrm{rms}} = \langle (\boldsymbol{U} - \overline{\boldsymbol{U}})^2 \rangle_{\mathrm{t}}^{1/2}$, with the average taken over the full volume as indicated by the angle brackets, and over the statistically steady part of the simulations, indicated by the subscript t. Our results are not sensitive to the relaxation time τ in the range $0.1 < \tau u_{\mathrm{rms}} k_{\mathrm{f}} < 10$ so the (arbitrary) choice $\tau u_{\mathrm{rms}} k_{\mathrm{f}} = 1$ is justified. We choose a simple harmonic form for the shear flow according to

$$\overline{U}_y^{(0)} = U_0 \cos(k_U z), \tag{5}$$

where U_0 is the flow amplitude, and $k_U = k_1, 2k_1, \ldots, k_U^{\max}$, $k_1 = 2\pi/L$.

2.2. Input and output quantities

We measure density in terms of its initially uniform value ρ_0, velocity in units of the sound speed c_{s}, and length in terms of k_1^{-1}. Furthermore, in the cases with the test-field method employed, we choose a system of electromagnetic units in which $\mu_0 = 1$, where μ_0 is the permeability of vacuum. The simulations are fully defined by choosing the forcing amplitude f_0 and scale k_{f}/k_1, kinematic viscosity ν, microscopic magnetic Prandtl number

$$\mathrm{Pm} = \frac{\nu}{\eta}, \tag{6}$$

where η is the microscopic magnetic diffusivity in the test-field method, and the shear parameter

$$\mathrm{Sh_c} = \frac{U_0 k_U}{c_{\mathrm{s}} k_{\mathrm{f}}}. \tag{7}$$

We further assume that the scale of the test fields always equals that of the imposed large-scale flow, that is $k_B = k_U$, and that the value of Pm for the test-field simulations equals unity. For the scale separation ratio $\mathscr{S}$ we employ the definition

$$\mathscr{S} = k_{\mathrm{f}}/k_U. \tag{8}$$

The following quantities are used as diagnostics of our models. We quantify the level of turbulence in the simulations by the fluid and magnetic Reynolds numbers

$$\mathrm{Re} = \frac{u_{\mathrm{rms}}}{\nu k_{\mathrm{f}}}, \quad \mathrm{Rm} = \frac{u_{\mathrm{rms}}}{\eta k_{\mathrm{f}}} = \mathrm{Pm}\,\mathrm{Re}. \tag{9}$$

The strength of the imposed shear is measured by the dynamic shear number

$$\mathrm{Sh} = \frac{U_0 k_U}{u_{\mathrm{rms}} k_{\mathrm{f}}}. \tag{10}$$

Guided by MLT and FOSA, we normalise both the turbulent viscosity and magnetic diffusivity by

$$\nu_{\mathrm{t0}} = \eta_{\mathrm{t0}} = u_{\mathrm{rms}}/3k_{\mathrm{f}}, \tag{11}$$

while the turbulent magnetic Prandtl number is given by

$$\mathrm{Pm_t} = \frac{\nu_{\mathrm{t}}}{\eta_{\mathrm{t}}}. \tag{12}$$

3. Computation of ν_{t} and η_{t}

3.1. Mean-field analysis

In what follows, we rely upon Reynolds averaging, specifically defining the mean quantities as averages over x and y. Hence, they can only depend on z and time. Averages are indicated by overbars and fluctuations by lowercase or primed quantities, thus $\boldsymbol{U} = \overline{\boldsymbol{U}} + \boldsymbol{u}$, $\rho = \overline{\rho} + \rho'$ etc.

3.1.1. Hydrodynamics

In the incompressible case all turbulent effects can be subsumed in the Reynolds stress tensor $Q_{ij} = \overline{u_i u_j}$ whose divergence appears in the evolution equation of the mean flow. Including compressibility and starting from

$$\partial_t(\rho U_i) + \partial_j(\rho U_i U_j) = -\partial_i P + \ldots, \tag{13}$$

where the dots stand for viscous and external forces, one obtains after averaging

$$\begin{aligned} \partial_t(\overline{\rho' u_i} + \overline{\rho}\,\overline{U}_i) & \\ + \partial_j(\overline{\rho}\,\overline{u_i u_j} + \overline{U}_i \overline{\rho' u_j} + \overline{U}_j \overline{\rho' u_i} + \overline{\rho' u_i u_j} + \overline{\rho}\,\overline{U}_i \overline{U}_j) & \\ = -\partial_i \overline{P} + \ldots . & \end{aligned} \tag{14}$$

The contributions proportional to the Reynolds stresses, $\overline{\rho}\,\overline{u_i u_j}$, no longer cover all turbulent effects originating from the inertial terms. However, in our weakly compressible setups with Ma ≈ 0.1 the difference between, for example $|\overline{(\rho u_y)' u_z}/\rho_0 u_{\mathrm{rms}}^2|$ and $|\overline{\rho}\,\overline{u_y u_z}/\rho_0 u_{\mathrm{rms}}^2|$ is $O(10^{-2})$[3]. Thus, we will consider, as in the incompressible case, only the Reynolds stresses[4]. When restricting to first order in the mean quantities, they can be decomposed into three contributions,

$$Q_{ij} = Q_{ij}^{(0)} + Q_{ij}^{(\overline{\ln \rho})} + Q_{ij}^{(\overline{U})} \tag{15}$$

where $Q_{ij}^{(0)}$ is already present in the absence of both a mean flow $\overline{\boldsymbol{U}}$ and a gradient of $\overline{\ln \rho}$, $Q_{ij}^{(\overline{\ln \rho})}$ is occurring due to the presence of $\boldsymbol{\nabla}\overline{\ln \rho}$, and $Q_{ij}^{(\overline{U})}$ occurs due to the presence of $\overline{\boldsymbol{U}}$ (for a justification see Appendix A). As in our simulations no significant $\boldsymbol{\nabla}\overline{\ln \rho}$ occurs, we disregard $Q_{ij}^{(\overline{\ln \rho})}$. Further, as the fluctuations are isotropically forced, the only non-zero components of $Q_{ij}^{(0)}$ are $Q_{xx}^{(0)} = Q_{yy}^{(0)} = Q_{zz}^{(0)}$. Apart from small fluctuations, they do not depend on z and thus do not act onto the mean flow. Note that due to the absence of a global rotation there is also no contribution of the Λ effect in Q_{ij}. In what follows we drop the superscript $(\overline{U})$ for brevity.

For sufficiently slowly varying mean flows and sufficient scale separation, Q_{ij} can be approximately represented by the truncated Taylor expansion

$$Q_{ij} = A_{ijk} \overline{U}_k + N_{ijkl} \overline{U}_{k,l}, \tag{16}$$

with the symmetry requirements

$$A_{ijk} = A_{jik}, \quad N_{ijkl} = N_{jikl}. \tag{17}$$

Here, A_{ijk} describes the AKA effect, while N_{ijkl} comprises turbulent viscosity (amongst other effects)[5]. For isotropic (and hence

---

[3] Neglecting density fluctuations may not be rigorously justified, given that the variety of potentially new effects owing to compressibility has not yet been fully explored, but see the recent studies by Rogachevskii et al. (2018) and Yokoi (2018) for the electromotive force. However, recent hydrodynamic results for the Λ effect suggest that the effect of compressibility is weak up to Ma ≈ 0.8 (Käpylä 2019b).

[4] Further turbulence effects result from the term $\overline{\mathbf{S} \cdot \boldsymbol{\nabla} \ln \rho}$, but are not considered here either because of our assumption of weak compressibility. We recall that $\mathbf{S}$ is the traceless rate of strain tensor used in Eq. (2).

[5] Note that relation (16) is yielding the stresses without truncation when interpreted to be a representation of the Fourier-transformed kernel of a general convolution-like relationship between Q_{ij} and $\overline{U}_j$ (cf. Brandenburg et al. 2008a).

homogeneous) fluctuations, that is in the kinematic limit $\overline{U} \rightarrow \mathbf{0}$, $A_{ijk} = 0$, and N_{ijkl} must have the form

$$N_{ijkl} = -\nu_t(\delta_{ik}\delta_{jl} + \delta_{il}\delta_{jk}) - \zeta_t \delta_{ij}\delta_{kl}, \tag{18}$$

where the constants ν_t and ζ_t are the turbulent shear and bulk viscosities, respectively. The Reynolds stresses appear then correspondingly as

$$Q_{ij} = -\nu_t(\overline{U}_{i,j} + \overline{U}_{j,i}) - \sigma_t \delta_{ij} \boldsymbol{\nabla} \cdot \overline{\boldsymbol{U}}, \tag{19}$$

with the first term reproducing the Boussinesq ansatz. Although our turbulence is isotropically forced, the presence of finite shear causes it to be anisotropic with preferred directions given by the direction of the mean flow $\overline{\boldsymbol{U}}$ and, say, its curl, $\overline{\boldsymbol{W}} = \boldsymbol{\nabla} \times \overline{\boldsymbol{U}}$. Given that it is the divergence of Q_{ij} which enters the mean momentum equation and mean quantities depend only on z, merely the components A_{i3k} and N_{i3k3} matter in (16). As $\overline{\boldsymbol{U}}$ needs not to be solenoidal, $\overline{U}_z$ might in general depend on z and the turbulent bulk viscosity is then of interest.

Further simplification is obtained when assuming that the mean velocity has only one component. In our setup, the mean flow is always very close to the maintained one, that is, $\overline{\boldsymbol{U}} \approx \overline{\boldsymbol{U}}^{(0)} \sim \boldsymbol{e}_y$. Then we have

$$Q_{i3} = A_{i32}\overline{U}_y + N_{i323}\overline{U}_{y,z} = a_i\overline{U}_y + n_i\overline{U}_{y,z}, \tag{20}$$

where we have introduced new coefficients $a_i = A_{i32}$ and $n_i = N_{i323}$. Comparison with (19) reveals that for $\overline{U}_y \rightarrow 0$ with isotropic forcing $n_2 \rightarrow -\nu_t$ while a_i and $n_{1,3}$ should approach zero.

We note that the AKA-effect can only be expected to appear in Galilean non-invariant flows (Frisch et al. 1987). This is not the case for the flows considered here, because the forcing is δ correlated in time, so there is no difference between a forcing defined in an arbitrary inertial frame and a forcing defined in the (resting) lab frame.

3.1.2. Magnetohydrodynamics

We consider only z dependent mean fields in which case the mean electromotive force $\overline{\mathcal{E}}$, when truncated in analogy to (16), can be represented by two rank–2 tensors

$$\overline{\mathcal{E}}_i = \alpha_{ij}\overline{B}_j - \eta_{ij}\overline{J}_j, \quad \overline{\boldsymbol{J}} = \boldsymbol{\nabla} \times \overline{\boldsymbol{B}}, \quad i, j = 1, 2, 3, \tag{21}$$

where $\boldsymbol{J} = \boldsymbol{\nabla} \times \boldsymbol{B}$ is the current density. Given that all quantities depend only on z, we have $\overline{J}_z = 0$ and because $\overline{B}_z = $ const. by virtue of $\boldsymbol{\nabla} \cdot \overline{\boldsymbol{B}} = 0$, $\overline{\mathcal{E}}_z(z)$ has no effect on the evolution of $\overline{\boldsymbol{B}}$. Hence we set $\overline{B}_z = 0$ and restrict our interest to the components α_{ij} and η_{ij} with $i, j = 1, 2$. As the pseudo-tensor α_{ij} can for non-helical forcing merely be constructed from the building blocks $\overline{U}_i$ and $\overline{W}_j$ by the products $\overline{U}_i\overline{W}_j$ and $\overline{U}_j\overline{W}_i$, within its restricted part, only the components α_{12} and α_{21} can be non-zero for our setup. Building blocks for the anisotropic part of the restricted η_{ij} are here

$$\overline{W}_i\overline{W}_j, \overline{U}_i\overline{U}_j, \quad \text{and higher order terms,} \tag{22}$$

hence the off-diagonal components $\eta_{12,21}$ need to vanish. So all the relevant components, except an isotropic contribution to $\boldsymbol{\eta}$, have leading order in U_0 of at least 2. In the limit $U_0 \rightarrow 0$ we have $\alpha_{ij} \rightarrow 0$ while $\eta_{11,22} \rightarrow \eta_t$.

3.2. Imposed shear method

We apply three methods to extract the mean-field coefficients from the simulation data:

M1: The mean flow $\overline{U}_y$ depends on z, and as it is approximately harmonic, its zeros do not coincide with those of its derivative $\overline{U}_{y,z} = -\overline{W}_x$. Hence the coefficients a_i and n_i can be isolated by

$$a_i\left(z_j^W, t\right) = Q_{iz}\left(z_j^W, t\right)/\overline{U}_y\left(z_j^W, t\right), \tag{23}$$

$$n_i\left(z_j^U, t\right) = -Q_{iz}\left(z_j^U, t\right)/\overline{W}_x\left(z_j^U, t\right), \tag{24}$$

where z_j^U and z_j^W are the zeros of $\overline{U}_y$ and $\overline{W}_x$, respectively. a_i and n_i are then further subjected to temporal averaging. In general, their values at the different zeros will only coincide in the limit $U_0 \rightarrow 0$, but in our case the differences turned out to be smaller than the error bars.

M2a: We use constant fit coefficients a_i and n_i in the time averaged simulation data of Q_{iz}, $\overline{U}_y$, and $\partial_z\overline{U}_y$:

$$Q_{iz} = a_i\overline{U}_y + n_i\partial_z\overline{U}_y. \tag{25}$$

M2b: Alternatively, we drop the non-diffusive contribution and use only a single coefficient n_i as a fit parameter:

$$Q_{iz} = n_i\partial_z\overline{U}_y. \tag{26}$$

For method M1 we divide the time series of a_i and n_i into three parts and define the largest deviation from the average, taken over the whole time series, as the error. For M2a,b we similarly perform the fit for data averaged over three equally long parts of the time series and take the error to be the largest deviation from the fitted values obtained from a time average over the full time series. Our results indicate that only the Reynolds stress component Q_{yz} shows a significant signal that can be related to the mean-field effects discussed above.

Figure 1 shows the horizontally averaged mean flow $\overline{U}_y(z, t)$, Reynolds stress component $Q_{yz}(z, t)$, and the z profiles of its temporal average along with $-\nu_t\overline{U}_{y,z}$ from method M2b. The imposed velocity profile induces a large-scale pattern in the Reynolds stress with the same vertical wavenumber, but with a vertical shift of $\pi/2$.

3.3. Decay experiments

Apart from measuring the response of the system to imposed shear, it is possible to measure the turbulent viscosity independently from the decay of large-scale flows. We refer to this procedure as M3. We employ this method to check the consistency of methods M1 and M2 in a few cases.

The dispersion relation for the large-scale flow $\overline{U}_y$ is given by

$$\omega = -\nu_T k_z^2, \tag{27}$$

where $\nu_T = \nu + \nu_t$ and k_z is the wavenumber of the flow. Equation (27) is valid if large-scale velocities other than $\overline{U}_y$, the pressure gradient, and the effects of compressibility are negligible. We measure the decay rate of the $k_z = k_U$ constituent of the flow by extracting its amplitude using Fourier transform and fitting an exponential function to the data. The clear exponential decay is drowned out by the random signal from the turbulence after a time that depends on the amplitude of the initial large-scale flow and other characteristics of the simulations. Thus we
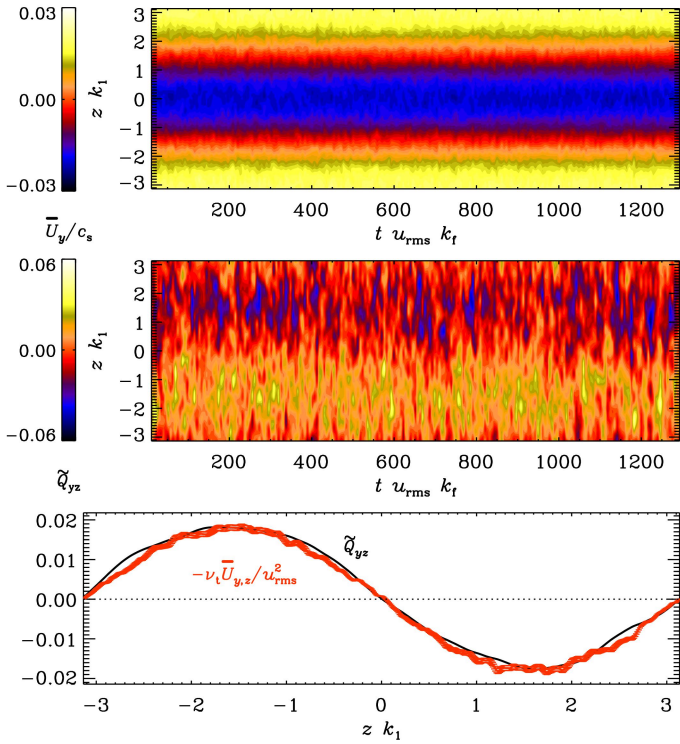
Fig. 1. Horizontally averaged velocity $\overline{U}_y(z,t)$ (*top*), $\tilde{Q}_{yz}(z,t) = Q_{yz}/u_{\rm rms}^2$ (*middle*), and its temporal average in comparison with $-\nu_{\rm t}\overline{U}_{y,z}/u_{\rm rms}^2$ (*bottom*) from Run E9 (see Table 2) with $\tilde{k}_{\rm f} = k_{\rm f}/k_1 = 5$, $\tilde{k}_U = k_U/k_1 = 1$, Sh ≈ 0.04, and Re ≈ 497. $\nu_{\rm t}$ from method M2b.

limit the fitting to the clearly decaying part of the time series which typically covers roughly 300 turnover times.

To reduce the effect of the stochastic fluctuations of the turbulence, we perform N independent realisations of the decay and measure $\nu_{\rm t}$ from the decay rate in each case. This is achieved by using N uncorrelated snapshots from the fiducial run with imposed shear flow as initial conditions for decay experiments, see Fig. 6 for representative results where $N = 10$. Such snapshots are separated by at least 80 turbulent eddy turnover times. An error estimate is obtained by dividing the obtained values of $\nu_{\rm t}$ into two groups and considering the largest deviation of averages over these from the average over the full set.

3.4. Test-field method

We use the test-field method, originally described in Schrinner et al. (2005, 2007), to determine the turbulent transport coefficients α_{ij} and η_{ij}. Our formulation is essentially the same as in Brandenburg et al. (2008b). The fluctuating magnetic fields are evolved with the flow taken from the simulation by

$$\frac{\partial \boldsymbol{a}^{\rm T}}{\partial t} = \overline{\boldsymbol{U}} \times \boldsymbol{b}^{\rm T} + \boldsymbol{u} \times \overline{\boldsymbol{B}}^{\rm T} + \left(\boldsymbol{u} \times \boldsymbol{b}^{\rm T}\right)' + \eta \nabla^2 \boldsymbol{a}^{\rm T}, \tag{28}$$

where $\boldsymbol{b}^{\rm T} = \boldsymbol{\nabla} \times \boldsymbol{a}^{\rm T}$, η is the magnetic diffusivity, and $\overline{\boldsymbol{B}}^{\rm T}$ is one out of a set of large-scale test fields. Neither the fluctuating fields $\boldsymbol{a}^{\rm T}$ nor the test fields $\boldsymbol{B}^{\rm T}$ act back on the flow. Each of the test fields yields an electromotive force (EMF)

$$\overline{\mathcal{E}} = \overline{\boldsymbol{u} \times \boldsymbol{b}^{\rm T}}. \tag{29}$$

Assuming that the mean field $\overline{\boldsymbol{B}}$ varies slowly in space and time, the electromotive force can be written as

$$\overline{\mathcal{E}}_i = \alpha_{ij}\overline{B}_j + \beta_{ijk}\frac{\partial \overline{B}_k}{\partial x_j}, \tag{30}$$

where α_{ij} and β_{ijk} represent the α effect and turbulent diffusion, respectively. These coefficients can be unambiguously inverted from Eq. (30) by choosing an appropriate number of independent test fields.

We use four stationary z dependent test fields

$$\overline{\boldsymbol{B}}^{1{\rm c}} = B_0(\cos k_B z, 0, 0), \quad \overline{\boldsymbol{B}}^{2{\rm c}} = B_0(0, \cos k_B z, 0), \tag{31}$$

$$\overline{\boldsymbol{B}}^{1{\rm s}} = B_0(\sin k_B z, 0, 0), \quad \overline{\boldsymbol{B}}^{2{\rm s}} = B_0(0, \sin k_B z, 0),$$

where k_B is a wavenumber. As explained in Sect. 3.1.2, Eq. (30) simplifies here to Eq. (21) with $\eta_{i1} = \beta_{i23}$ and $\eta_{i2} = -\beta_{i13}$. Because of $\alpha_{11,22} = 0$, $\alpha_{12,21} \to 0$ for $U_0 \to 0$ we neglect the latter for weak imposed shear flows and simplify Eq. (21) further to

$$\overline{\mathcal{E}}_i = -\eta_{ij}\overline{J}_j. \tag{32}$$

We are interested in the diagonal components of η_{ij} which we represent in terms of the turbulent diffusivity by

$$\eta_{\rm t} = \tfrac{1}{2}(\eta_{11} + \eta_{22}). \tag{33}$$

In the case of homogeneous isotropic turbulence, the turbulent transport coefficients are uniform across the system and volume averages are appropriate. In the present case, however, the turbulence can neither be considered fully isotropic nor homogeneous due to the imposed z dependent shear flow, which makes the coefficients also anisotropic and z dependent. Both effects are weak though in the computed $\eta_{\rm t}$; see Sect. 4.2 for the effect of anisotropy.

Exponential growth of the test solutions $\boldsymbol{b}^{\rm T}$ at high Rm is a known issue in the test-field method (Sur et al. 2008). To circumvent it, we reset the $\boldsymbol{b}^{\rm T}$ periodically to zero with a resetting time that is roughly inversely proportional to the magnetic Reynolds number.

The error of the turbulent magnetic Prandtl number is computed from

$$\delta{\rm Pm}_{\rm t} \approx {\rm Pm}_{\rm t}\left(\frac{\delta\nu_{\rm t}}{\nu_{\rm t}} + \frac{\delta\eta_{\rm t}}{\eta_{\rm t}}\right), \tag{34}$$

where $\delta\nu_{\rm t}$ and $\delta\eta_{\rm t}$ are the errors of turbulent viscosity and diffusivity, respectively.

4. Results

We perform several sets of simulations where we vary the forcing wavenumber $k_{\rm f}$, determining the scale separation ratio, fluid and magnetic Reynolds numbers Re and Rm, respectively, and the wavenumber of the large-scale flow k_U. Representative examples of the flow patterns realised in runs with small, medium, and high Reynolds numbers (from left to right) and forcing wavenumbers $\tilde{k}_{\rm f} = (3, 5, 10, 30)$ (from top to bottom, Sets D−G) are shown in Fig. 2. We also typically evolve the test-field equations in our runs so the results pertaining to $\nu_{\rm t}$ and $\eta_{\rm t}$ are always obtained from the same simulation. All of our runs are listed in Tables 1–3.

In Fig. 3 we show representative results for a_2 and $\nu_{\rm t}$ obtained with the methods M1 and M2a from Sets A–C (see Table 1)
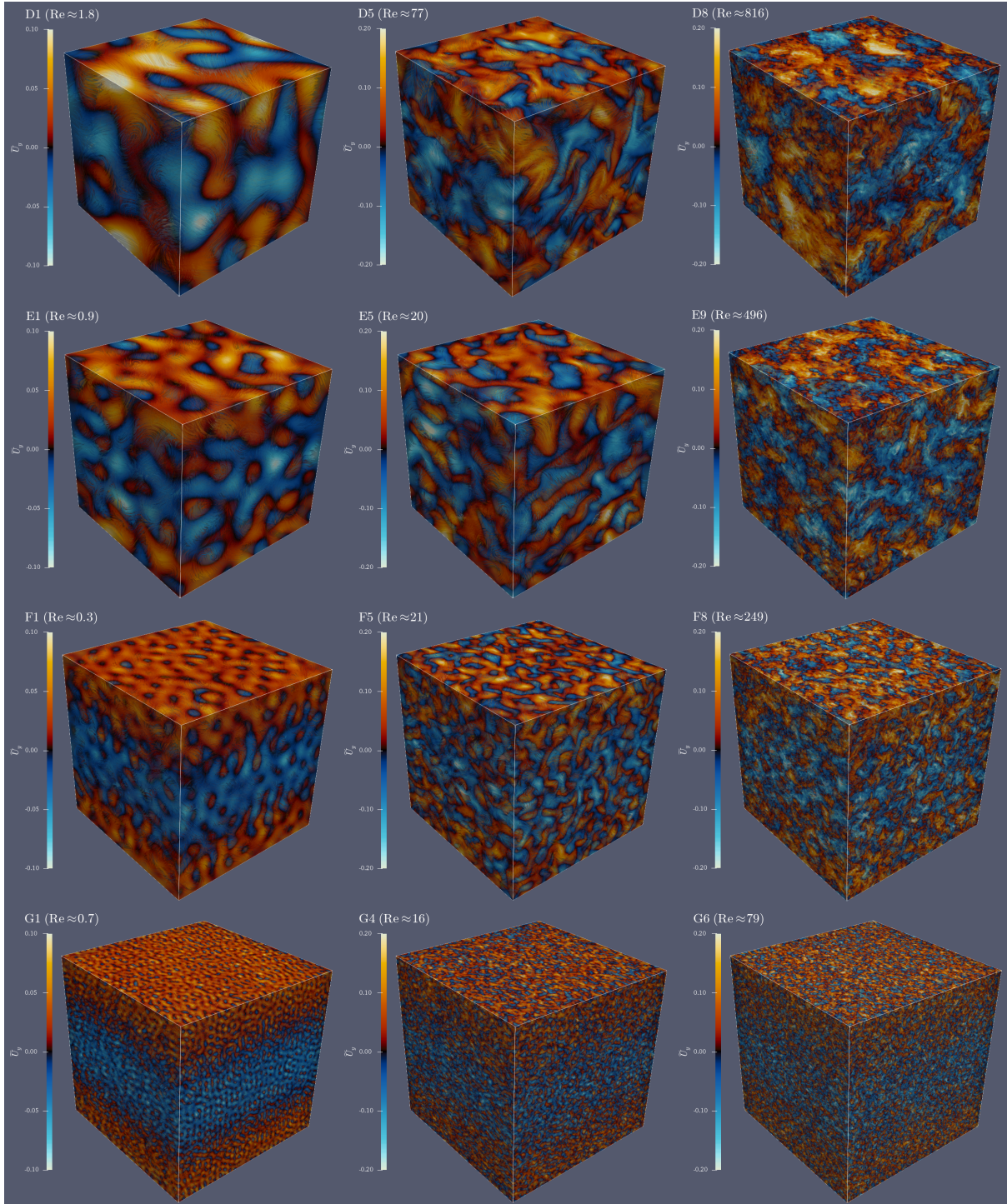
Fig. 2. Normalised streamwise velocity component $\tilde{U}_y = U_y/c_s$ at the periphery of the computational domain for increasing scale separation ratio (*from top to bottom*), and increasing Reynolds number (*left to right*) for selected runs from D1 to G6.

with forcing wavenumbers 3, 5, and 10. The coefficient a_2, corresponding to the AKA-effect, is consistent with zero for all values of shear and with both methods that can detect it. This conclusion applies to all of our models and is consistent with the Galilean invariance of our forcing.

We note that, as a_2 from method M2a is always very small, it has a negligible effect on the quality of the fit and the value of ν_t in comparison to method M2b. For simplicity, we present results obtained using M2b in what follows. Overall, no statisti-

cally significant values were obtained for the coefficients a_1, a_3, n_1, and n_3.

4.1. Turbulent viscosity

4.1.1. Dependence on position and sensitivity to shear

The turbulent viscosities obtained for the two zeros employed in M1 (M1$_1$ and M1$_2$ in Fig. 3) agree within error estimates and agree also with those obtained from M2a and M2b. This suggests
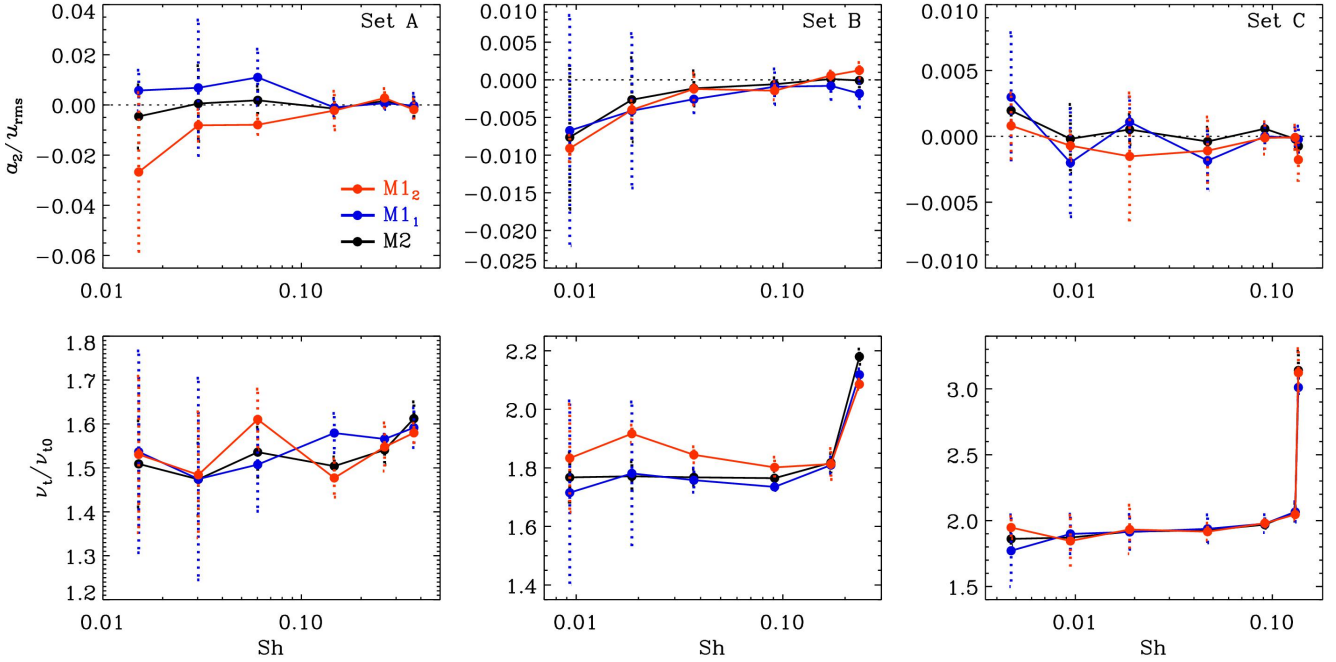
Fig. 3. AKA–effect coefficient a_2 (*top*) and turbulent viscosity ν_t (*bottom*) as functions of Sh for three scale separation ratios, $\mathscr{S} = 3$ (Set A, *left*), 5 (Set B, *middle*), and 10 (Set C, *right*). The colours refer to methods M1 (blue and red), and M2a (black). $M1_1$ and $M1_2$ refer to the two zeros employed in Eqs. (23) and (24).

Table 1. Summary of the runs with varying shear.

Run	Re	Sh	Sh_c [10^{-5}]	$\tilde{k}_f$	Ma	$\tilde{\nu}_t$	$\tilde{\eta}_t$	Pm_t	Grid
A1	21	0.015	160	3	0.105	1.509	1.899	0.795	72^3
A2	21	0.030	319	3	0.106	1.566	1.873	0.836	72^3
A3	21	0.060	638	3	0.106	1.575	1.912	0.824	72^3
A4	22	0.146	1595	3	0.109	1.452	1.900	0.764	72^3
A5	25	0.264	3191	3	0.121	1.496	2.098	0.713	72^3
A6	35	0.369	6381	3	0.173	1.618	2.192	0.738	72^3
B1	21	0.009	98	5	0.105	1.768	2.018	0.876	144^3
B2	21	0.019	196	5	0.105	1.699	2.031	0.836	144^3
B3	21	0.037	392	5	0.106	1.769	2.097	0.844	144^3
B4	21	0.091	981	5	0.107	1.760	2.083	0.845	144^3
B5	23	0.171	1962	5	0.115	1.818	2.361	0.770	144^3
B6	33	0.235	3923	5	0.167	2.180	4.048	0.538	144^3
C1	21	0.005	50	10	0.106	1.856	2.110	0.880	144^3
C2	21	0.009	100	10	0.106	1.905	2.113	0.901	144^3
C3	21	0.019	199	10	0.106	1.916	2.136	0.897	144^3
C4	21	0.047	499	10	0.106	1.926	2.216	0.869	144^3
C5	22	0.092	997	10	0.109	1.969	2.450	0.804	144^3
C6	23	0.131	1496	10	0.115	2.063	2.811	0.734	144^3
C7	29	0.136	1994	10	0.147	3.140	5.037	0.623	144^3

Notes. Ma $= u_{rms}/c_s$ is the Mach number, $\tilde{\nu}_t = \nu_t/\nu_{t0}$, and $\tilde{\eta}_t = \eta_t/\eta_{t0}$. Furthermore, $\tilde{k}_B = \tilde{k}_U = 1$ in all runs yielding $\mathscr{S} = \tilde{k}_f$. Here and in subsequent tables, ν_t is measured with method M2b and η_t with the test-field method.

that ν_t has only a weak dependence on z or that its spatial profile is such that it is not captured by this method.

When the amplitude of the shear flow is varied, the values of ν_t start to increase rapidly at the largest values of Sh; see Fig. 3. This is because the Navier–Stokes equations are inherently non-linear. Therefore, imposing a large-scale flow has an impact on the turbulence. However, if the shear is sufficiently weak, such feedback is small and reliable results for ν_t can be obtained. To assess this question, we perform simulations at fixed kinematic viscosity and given forcing wavenumber k_f while varying the

shear systematically. With the other quantities held unchanged, the fluid Reynolds number is a measure of the rms–velocity of the turbulence. In Fig. 4, we show the Reynolds numbers realised in the same sets as in Fig. 3. We find that Re increases mildly as a function of Sh for weak shear (Sh $\lesssim$ 0.1) and starts to increase sharply at higher values while the location of the transition depends weakly on the forcing wavenumber such that the larger the k_f, the smaller Sh is needed for the increase to occur.

The increase of Re is due to the fact that the turbulence becomes increasingly affected by the imposed shear and attains significant anisotropy. In some cases with the highest values of Sh, we also see large-scale vorticity generation, which is likely related to what is known as vorticity dynamo (e.g. Käpylä et al. 2009b). Such hydrodynamic instability can be excited by the off-diagonal components of the turbulent viscosity tensor in anisotropic turbulence in the presence of shear (Elperin et al. 2003, 2007).

These tests suggest that values of Sh below 0.1 are needed for the influence of the shear on the turbulence to remain weak. However, the excitation condition of the vorticity dynamo manifestly depends on the scale separation ratio and likely also on the Reynolds number. In our runs, we choose a constant value of Sh_c for which Sh remains clearly below the excitation threshold (note that Sh_c = Sh Ma). Another factor supposedly contributing at large Reynolds numbers is shear-produced turbulence – possibly through some sort of finite amplitude instability. Given that the shear strengths (in terms of Sh) considered here are relatively small, this effect is likely to be weak in comparison to the turbulence production due to the applied forcing.

4.1.2. Dependence on Re

Results for the turbulent viscosity as a function of the fluid Reynolds number are shown in Fig. 5 for Sets D–G (see Table 2). Here the value of the shear parameter Sh_c is constant in each set.

**Table 2.** Summary of the runs with varying Reynolds numbers.

Run	Re	Sh	Sh_c [10^{-5}]	$\tilde{k}_f$	Ma	$\tilde{\nu}_t$	$\tilde{\eta}_t$	Pm_t	Grid
D1	1.8	0.144	813	3	0.056	0.505	0.857	0.589	64^3
D2	4.9	0.106	813	3	0.077	1.068	1.594	0.670	64^3
D3	16	0.080	813	3	0.101	1.481	1.896	0.781	64^3
D4	36	0.071	813	3	0.114	1.508	1.832	0.823	64^3
D5	77	0.067	813	3	0.121	1.430	1.735	0.824	128^3
D6	198	0.065	813	3	0.124	1.329	1.590	0.836	128^3
D7	401	0.065	813	3	0.126	1.247	1.551	0.804	256^3
D8	816	0.064	813	3	0.128	1.310	1.489	0.880	512^3
E1	0.9	0.112	500	5	0.045	0.242	0.447	0.540	64^3
E2	1.5	0.094	500	5	0.053	0.434	0.762	0.570	64^3
E3	2.4	0.080	500	5	0.062	0.702	1.182	0.594	64^3
E4	8.8	0.056	500	5	0.089	1.468	2.007	0.732	64^3
E5	20	0.047	500	5	0.106	1.665	2.020	0.824	64^3
E6	45	0.043	500	5	0.117	1.693	1.901	0.891	128^3
E7	121	0.040	500	5	0.124	1.578	1.733	0.911	256^3
E8	246	0.040	500	5	0.125	1.485	1.678	0.885	256^3
E9	497	0.039	500	5	0.127	1.382	1.604	0.862	512^3
F1	0.3	0.080	254	10	0.032	0.096	0.156	0.617	128^3
F2	0.9	0.057	254	10	0.045	0.274	0.454	0.603	128^3
F3	3.4	0.037	254	10	0.069	1.049	1.532	0.685	128^3
F4	8.9	0.028	254	10	0.089	1.670	2.103	0.794	128^3
F5	21	0.024	254	10	0.106	1.905	2.116	0.900	128^3
F6	59	0.021	254	10	0.119	1.787	1.926	0.928	256^3
F7	123	0.021	254	10	0.123	1.700	1.802	0.943	512^3
F8	249	0.020	254	10	0.125	1.607	1.712	0.939	512^3
G1	0.7	0.021	84	30	0.041	0.205	0.356	0.577	288^3
G2	1.9	0.015	84	30	0.058	0.675	1.114	0.606	288^3
G3	5.2	0.011	84	30	0.078	1.429	2.090	0.684	288^3
G4	16	0.008	84	30	0.102	1.930	2.215	0.871	288^3
G5	38	0.007	84	30	0.114	1.915	2.072	0.924	576^3
G6	79	0.007	84	30	0.120	1.856	1.844	1.007	576^3

Notes. All quantities have the same meanings as in Table 1. Again $\tilde{k}_B = \tilde{k}_U = 1$ and $\mathscr{S} = \tilde{k}_f$.

Additionally, the normalized relaxation time $\tau u_{rms} k_f = 1$ is kept fixed by adjusting τ, and $\tilde{k}_f$ is varied between 3 (Set D) and 30 (Set G). Furthermore, these runs use $\tilde{k}_U = \tilde{k}_B = 1$.

We find that for low Re and poor scale separation the signal is noisy and produces large errors in ν_t unless very long time series are produced. The runs with $k_f \approx 3$ and Re ≈ 1 were in all sets typically run for several thousand turnover times whereas for larger Reynolds numbers and scale separations the integration times can be an order of magnitude shorter. The results in the low Reynolds number regime are in agreement with $\nu_t \propto$ Re as expected from analytic studies using FOSA (Krause & Rüdiger 1974). The value of ν_t increases until Re ≈ 10 after which it saturates roughly to a constant between one and two times ν_{t0} depending on the scale separation ratio $\mathscr{S}$. However, we still see a slow decrease for the highest values of Re which likely indicates that even the highest resolution simulations are not in the regime of fully developed turbulence. We note that the Mach number changes by a factor between roughly two (Set D) to four (Set F) between the extreme runs in each set. However, Ma saturates in the high-Re runs so compressibility effects are unlikely to explain the slow declining trend of ν_t.

There is also a dependence on the scale separation ratio such that higher values of $\mathscr{S}$ result in larger values of $\tilde{\nu}_t$. In theory ν_t should converge towards the value at infinite scale separation. This is confirmed by Sets F and G where $\tilde{k}_f = 10$ and 30, respectively.
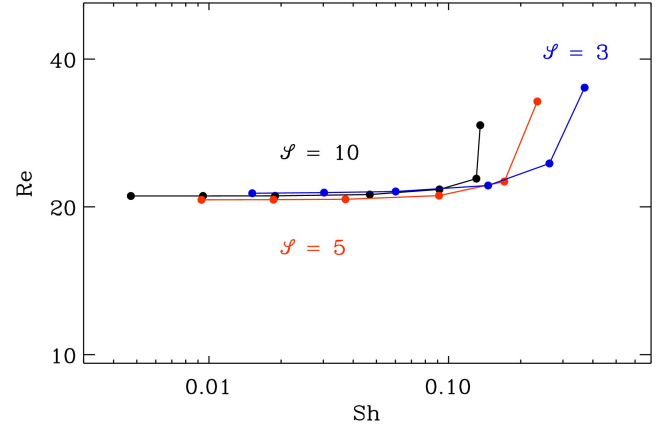
Fig. 4. Reynolds number as a function of Sh for three scale separation ratios, $\mathscr{S} = 3$ (blue), 5 (red), and 10 (black), or Sets A, B, and C, respectively.
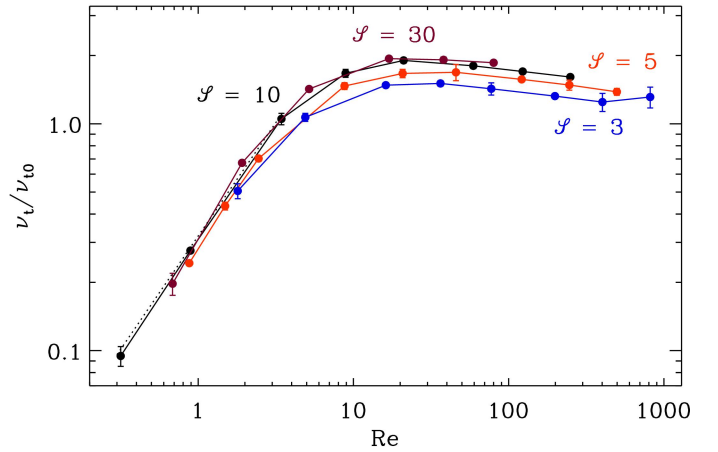
Fig. 5. Turbulent viscosity ν_t, normalised by ν_{t0}, as a function of the Reynolds number Re for sets of runs with different scale separation ratio $\mathscr{S}$, but $Sh_c = $ const. within each of the Sets D (blue), E (red), F (black), and G (purple). The dotted black line is proportional to Re.

4.1.3. Results from M3

As a representative example, Fig. 6 shows the decay of the $k = k_1$ constituent of $\overline{U}_y$ for ten independent initial conditions derived from Run F8. We compare the results for ν_t from methods M2b and M3 in Fig. 7 for Sets F and Fd. The runs of the latter were set up such that $N = 10$ snapshots from each of the runs in Set F with imposed shear were used as initial conditions. Thus each run in Set F works as a progenitor to ten decay experiments with the same system parameters in Set Fd. We find that the results from methods M2b and M3 coincide within the error estimates for low and intermediate Reynolds numbers (Re $\lesssim 20$). However, there is a systematic tendency for the ν_t from the decay experiments to exceed the value from the Reynolds stress method for Re $\gtrsim 30$ by 10–20%.

4.1.4. Dependence on scale separation ratio

The dependence of ν_t on the scale separation ratio $\mathscr{S}$ for four different forcing scales is given in Table 3 (Sets H–K). We fit the data to a Lorentzian as a function of the inverse scale separation ratio $\mathscr{S}^{-1}$

Table 3. Summary of the runs with varying scale separation ratio $\mathscr{S} = k_f/k_U$.

Run	Re	Sh	Sh_c [10^{-4}]	$\tilde{k}_f$	$\mathscr{S}$	Ma	$\tilde{\nu}_t$	$\tilde{\eta}_t$	Pm_t	Grid
H1	20	0.077	81	3	3.0	0.106	1.517	1.894	0.801	144^3
H2	20	0.153	163	3	1.5	0.106	1.101	1.477	0.746	144^3
H3	20	0.229	244	3	1.0	0.106	0.784	1.168	0.671	144^3
I1	20	0.047	50	5	5.0	0.106	1.705	2.037	0.837	144^3
I2	20	0.094	100	5	2.5	0.107	1.436	1.782	0.806	144^3
I3	20	0.140	150	5	1.7	0.107	1.120	1.538	0.728	144^3
I4	20	0.187	200	5	1.3	0.107	0.942	1.337	0.704	144^3
J1	21	0.024	25	10	10	0.106	1.883	2.142	0.879	144^3
J2	21	0.048	51	10	5.0	0.106	1.790	2.009	0.891	144^3
J3	21	0.072	76	10	3.3	0.106	1.584	1.899	0.834	144^3
J4	21	0.095	102	10	2.5	0.107	1.421	2.111	0.673	144^3
J5	21	0.119	127	10	2.0	0.107	1.265	1.635	0.774	144^3
J6	21	0.166	178	10	1.4	0.107	1.015	1.396	0.727	144^3
K1	16	0.008	8.4	30	30	0.102	1.930	2.215	0.871	288^3
K2	17	0.016	17	30	15	0.103	4.343	6.481	0.670	288^3
K3	16	0.025	25	30	10	0.102	1.981	2.286	0.867	288^3
K4	16	0.042	42	30	6.0	0.102	1.790	2.096	0.854	288^3
K5	17	0.083	85	30	3.0	0.103	1.512	1.855	0.815	288^3
K6	17	0.123	127	30	2.0	0.103	1.247	1.628	0.766	288^3
K7	17	0.164	170	30	1.5	0.103	1.057	1.426	0.741	288^3

Notes. All quantities have the same meanings as in Table 1.

$$\nu_t(k_U/k_f) = \frac{\nu_t(0)}{1 + \sigma(k_U/k_f)^2} = \frac{\nu_t(0)}{1 + \sigma\mathscr{S}^{-2}}, \tag{35}$$

where $\nu_t(0)$ and σ are fit parameters[6]. We also fit the data to a more general function where the exponent c of k_U/k_f is another fit parameter:

$$\nu_t(k_U/k_f) = \frac{\nu_t(0)}{1 + \sigma(k_U/k_f)^c} = \frac{\nu_t(0)}{1 + \sigma\mathscr{S}^{-c}}. \tag{36}$$

The inverse relative errors $\nu_t/\delta\nu_t$ are used as weights in the fit. The data and the fits are shown in Fig. 8. While the data is in reasonable agreement with a Lorentzian with $\nu_t(0) = 1.90$ and $\sigma = 1.80$, the more general function with $\nu_t(0) = 2.00$, $\sigma = 1.61$, and $c = 1.44$ yields a somewhat better fit. Data consistent with Lorentzian behaviour has been found earlier for η_t in low Reynolds number turbulence (Brandenburg et al. 2008a); see Table 4 for an overview of the σ values found previously in various cases ranging from magnetic diffusion in isotropic turbulence to passive scalar diffusion in shear flows, in which σ was typically below unity. However, a value of c close to 4/3, as found here, is indeed expected for fully developed Kolmogorov turbulence; see the discussion in the conclusions of Madarassy & Brandenburg (2010).

Note that σ was found to be larger under the second-order correlation approximation (SOCA), but the reason for this departure is unclear. Also, looking at Table 4, there is no obvious connection between the values of σ in different physical circumstances. More examples are needed to assess the robustness of the results obtained so far.

Knowing the value of σ is important for more accurate mean-field modelling. In physical space, a prescription like Eq. (35) corresponds to a convolution, which makes the Reynolds stress at a given position dependent on the mean velocity within a certain neighbourhood. In that way, non-locality is modelled.

---

[6] The parameter σ determines the intersection position of the asymptotics $\nu_t(0)$ and $\nu_t(0)\mathscr{S}^2/\sigma$, where ν_t becomes $\nu_t(0)/2$, as $\mathscr{S} = \sqrt{\sigma}$.
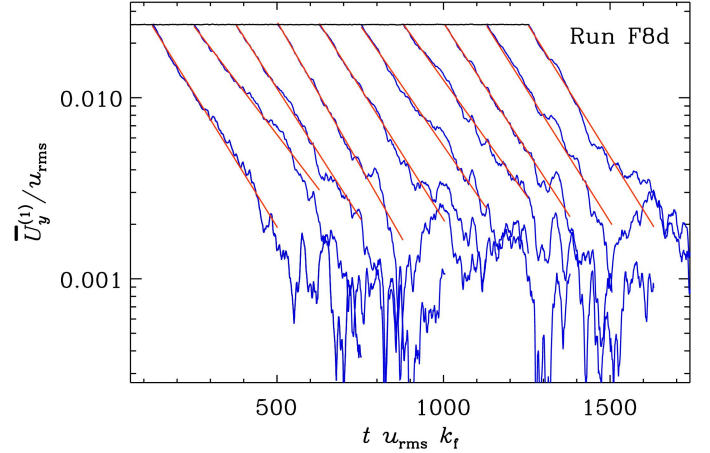
Fig. 6. Amplitude of the $k = k_1$ constituent of $\overline{U}_y(z, t)$ normalised by u_{rms} in Run F8d as a function of time from ten independent realisations of the decay. The solid red lines show exponential fits to the data.
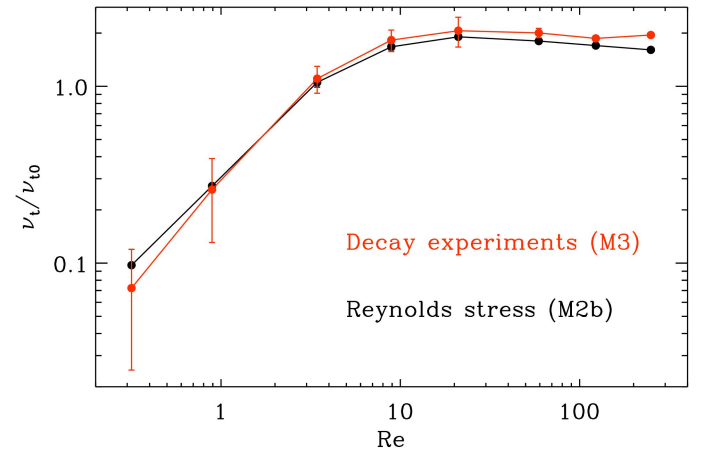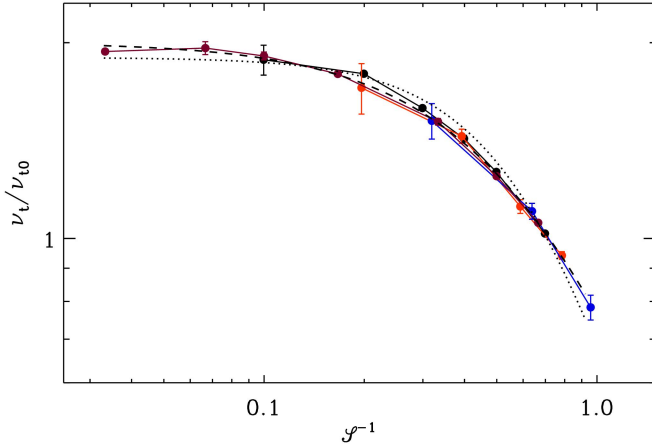

Fig. 7. Turbulent viscosity as a function of Re from method M2b, Set F (black) and from corresponding decay experiments (method M3), Set Fd (red).

This is generally ignored in the common use of turbulent viscosity, although some attempts have been made to include such affects to leading order (Rüdiger 1982). Ignoring non-locality corresponds to the limit $\sigma \to 0$ or $k_U/k_f \to 0$, which is often a questionable assumption; see Brandenburg & Chatterjee (2018) for a discussion in the context of spherical mean-field dynamos.

4.2. Turbulent diffusivity η_t

The turbulent magnetic diffusivity η_t from Sets D–G is shown in Fig. 9. We find a similar qualitative behaviour as for ν_t so that for small magnetic Reynolds numbers the value of η_t is proportional to Rm and the results converge when the scale separation ratio is increased. As in the case of the turbulent viscosity, we find a weak declining trend as a function of Rm at its highest values which was neither observed by Sur et al. (2008) in similar simulations without shear nor by Brandenburg et al. (2008b) and Mitra et al. (2009) in runs where the large-scale flow was imposed via the shearing-box approximation. However, the error estimates in the aforementioned studies are clearly greater than in the present one and thus a weak decreasing trend as a function of Rm cannot be

Fig. 8. Turbulent viscosity as a function of the inverse scale separation ratio k_U/k_f for the four normalised forcing wavenumbers $\tilde{k}_f = 3$ (blue), 5 (red), 10 (black), and 30 (purple), corresponding to Sets H–K, respectively. Fits according to Eqs. (35) and (36) are shown by dotted and dashed lines, respectively.

Table 4. Examples of σ values found previously in other cases.

σ	Case	References
0.16	Shear flow, passive scalar	Madarassy & Brandenburg (2010)
0.38	Passive scalar	Brandenburg et al. (2009)
0.25	Roberts flow, η_t, non-SOCA	Brandenburg et al. (2008a)
1	Roberts flow, α & η_t, SOCA	Brandenburg et al. (2008a)
1.80	ν_t, isotropic turbulence	Present work

ruled out. Furthermore, the shear flows in the present simulations are significantly weaker than in the cases of Brandenburg et al. (2008b) and Mitra et al. (2009), such that their influence on the turbulent transport coefficients is also weaker.

We assess the effect of the shear flow on the results by performing an additional set of simulations in which it is omitted, but otherwise the same parameters as in Set F are employed. We show the results for the difference of η_t in these sets in Fig. 10. The difference is typically of the order of a few per cent such that in most cases the value from the case with shear is greater. This is of the same order of magnitude as the error estimates for η_t. Thus we conclude that the systematic error due to the large-scale anisotropy induced by the shear flow is insignificant in the determination of the turbulent diffusivity.

4.3. Turbulent magnetic Prandtl number

Our results for Pm_t as a function of Reynolds number and scale separation ratio $\mathscr{S}$ are shown in Fig. 11. We find that Pm_t for $Re \gtrsim 20$ is roughly a constant for each value of $\tilde{k}_f$ while increasing from roughly 0.8 for $\tilde{k}_f = 3$ to 0.95 for $\tilde{k}_f = 10$. Especially at low Re, the convergence with respect to the scale separation is not as clear as for ν_t and η_t individually. With respect to low Reynolds numbers, we see an increasing trend starting from values between 0.55 and 0.65 at Re ≈ 5 until Re ≈ 20. At even lower Re the uncertainty in the determination of ν_t becomes larger and the values of Pm_t have substantial error margins.

The turbulent magnetic Prandtl number has been computed with various analytical techniques, see Table 5. Considering the limit of $\nu \to 0$ or Re $\to \infty$, different flavours of FOSA yield either $Pm_t = 0.8$ (Kitchatinov et al. 1994) or 0.4 (Yousef et al. 2003), whereas MTA results for fully developed turbulent con-
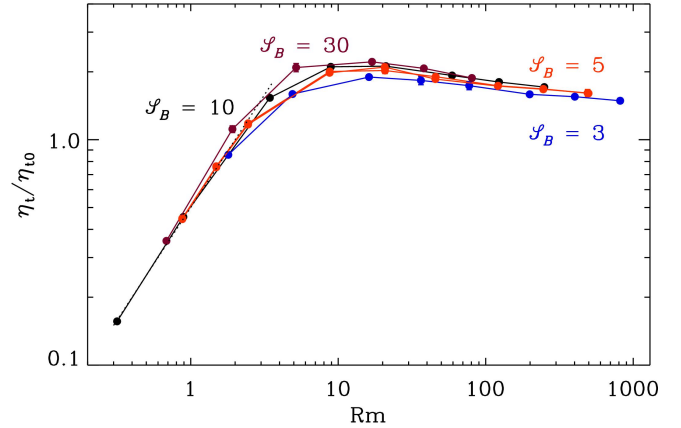
Fig. 9. Turbulent diffusivity η_t, normalised by η_{t0}, as a function of the magnetic Reynolds number Rm for runs with $Sh_c = \text{const.}$ within each of the Sets D (blue), E (red), F (black), and G (purple). The dotted black line is proportional to Rm and $\mathscr{S}_B = k_f/k_B$.
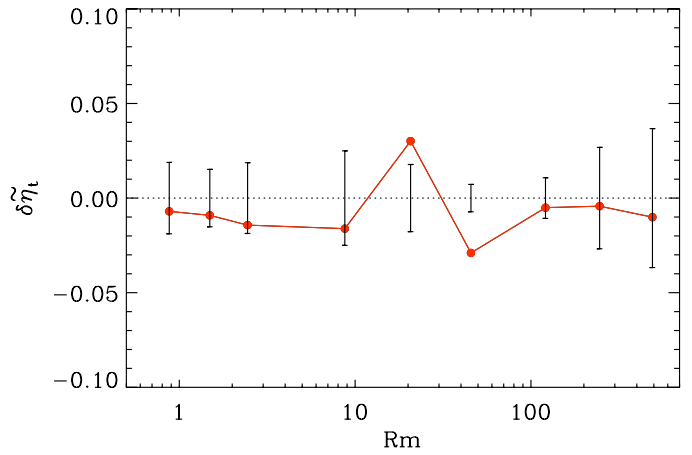

Fig. 10. Relative difference $\delta\tilde{\eta}_t = (\eta_t^{(0)} - \eta_t)/\eta_t$ of turbulent magnetic diffusivity from Set F and a corresponding set without shear, here denoted by superscript zero. The vertical bars indicate the error estimates of $\tilde{\eta}_t$ from Set F.

vection favours lower values (Rogachevskii & Kleeorin 2006). A similar spread of values from $Pm_t \approx 0.42$ (Verma 2001) to $\approx 0.7-0.8$ (Fournier et al. 1982; Kleeorin & Rogachevskii 1994; Jurčišinová et al. 2011) has been reported using renormalisation group methods for the case of three spatial dimensions and weak magnetic fields.

Particularly at high scale separation, our results are not compatible with any of the analytic results but indicate a higher value than all of the theories. This can be due to the fact that the turbulence in the simulations is not in the fully developed regime and because the scale separation achieved is still insufficient. Furthermore, analytic theories must resort to approximations that cannot be justified in high-Reynolds number turbulence.

4.4. Dependence on forcing time scale

The bulk of the simulations considered here use a δ correlated random (white) forcing, see Eq. (3), such that a new wavevector is chosen at every time step. It cannot, however, be ruled out a priori that the results depend on the correlation time of the forcing. Here we test the sensitivity of the results with respect to this correlation time by comparing the default case of white–in–time
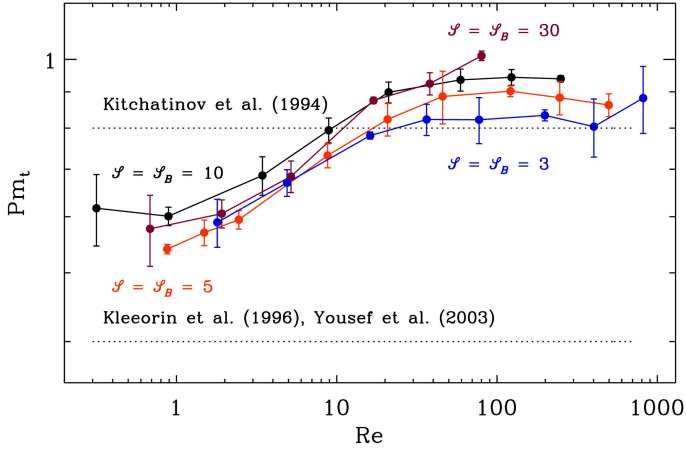
Fig. 11. Turbulent magnetic Prandtl number Pm_t as a function of the Reynolds number Re for the same sets of runs as in Fig. 6. Pm = 1 is used in all runs. The dotted horizontal lines indicate the extrema of analytical results from different methods; see Table 5.

Table 5. Comparison of values of Pm_t from analytic and numerical studies.

Pm_t	Method	References
0.4	FOSA	Yousef et al. (2003)
0.8	FOSA	Kitchatinov et al. (1994)
0.23–0.46	Spectral MTA, convect.	Rogachevskii & Kleeorin (2006)
≈ 0.72	Renormalisation group	Fournier et al. (1982)
≈ 0.79	Renormalisation group	Kleeorin & Rogachevskii (1994)
≈ 0.42	Renormalisation group	Verma (2001)
≈ 0.71	Renormalisation group	Jurčišinová et al. (2011)
≈ 1	DNS, dec. MHD turb.	Yousef et al. (2003)
≈ 0.9	DNS, high Re	Present work
0.55–0.65	DNS, low Re	Present work

forcing with cases where the forcing wavevector is held constant for a time δt_f. We take Run C4 as our fiducial model where $\delta t_f k_f u_{rms} \approx 0.02$ and δt_f is equal to the time step of the simulation. We increased $\delta t_f k_f u_{rms}$ in steps by a factor of 50 altogether and computed turbulent viscosity, magnetic diffusivity, and magnetic Prandtl number; see Fig. 12. We find that ν_t, η_t, and Pm_t are essentially constant in this range of parameters. Our method of switching the forcing with a period δt_f is crude because it induces discontinuities, but the approximate constancy of the coefficients suggests that robust results for the turbulent transport coefficients are obtained nevertheless.

5. Conclusions

We have computed the turbulent viscosity (ν_t) and magnetic diffusivity (η_t) from simulations of forced turbulence using imposed shear flows and the test-field method, respectively. As expected, ν_t and η_t are found to be proportional to the respective Reynolds number at low Re and Rm. With increasing values of Re and Rm, the turbulent transport coefficients saturate at around Re $\approx$ Rm $\approx$ 10, but show a weakly decreasing trend beyond. The value of the turbulent viscosity estimated from the Reynolds stress, which is interpreted to reflect the response of the system to a large-scale flow, and from the decay of a mean flow in the presence of turbulence are in fair agreement. However, the latter yields systematically slightly higher values for high Reynolds numbers by less than 10%.
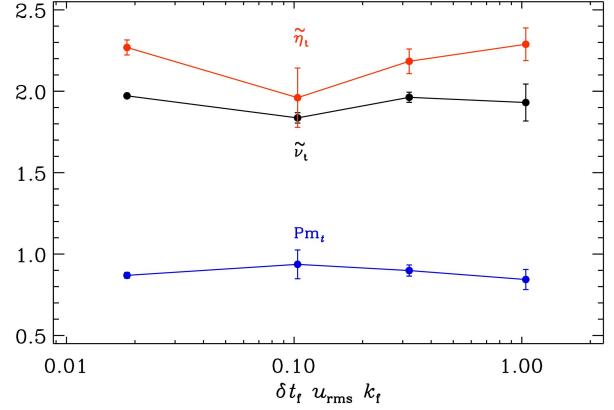
Fig. 12. Coefficients ν_t (black) and η_t (red), normalised by ν_{t0} and η_{t0}, respectively; and Pm_t (blue) as functions of $\delta t_f k_f u_{rms}$ using Run C4 as the fiducial model.

The turbulent magnetic Prandtl number Pm_t saturates between 0.8 and 0.95 for Re $\gtrsim$ 10 depending on the scale separation ratio. We note that these values are somewhat higher than those from the renormalisation group approach and, especially, the first-order smoothing approach. The value of Pm_t computed here corresponds to the kinematic case where the magnetic field is weak, which is often not the case in astrophysical systems. Analytic studies predict quenching of turbulent viscosity and magnetic diffusivity when the magnetic fields are dynamically significant (e.g. Kitchatinov et al. 1994). The quenching of η_t has also been computed from numerical simulations (e.g. Käpylä & Brandenburg 2009; Brandenburg et al. 2008c; Karak et al. 2014). Similar studies for turbulent viscosity are so far lacking. Such results will be reported elsewhere.

One of the other remaining issues to be addressed in the future is the role of compressibility effects, in particular that of fluctuations of ρ. In addition to making analytic progress by identifying potentially new effects owing to their presence, it would be useful to extend our simulations to the regime of larger Mach numbers. Another possible extension of our work is to study the potential of a small-scale dynamo to give rise of magnetic stresses that could enhance the turbulent viscosity, as has been suggested in the solar context to alleviate the discrepancies between observations and simulations of differential rotation and convective velocities (Karak et al. 2018).

References

Blandford, R. D., & Payne, D. G. 1982, MNRAS, 199, 883
Brandenburg, A., & Chatterjee, P. 2018, Astron. Nachr., 339, 118
Brandenburg, A., & Subramanian, K. 2005, Phys. Rep., 417, 1
Brandenburg, A., & von Rekowski, B. 2001, A&A, 379, 1153
Brandenburg, A., Tuominen, I., Moss, D., & Rüdiger, G. 1990, Sol. Phys., 128, 243
Brandenburg, A., Rädler, K.-H., & Schrinner, M. 2008a, A&A, 482, 739

Brandenburg, A., Rädler, K.-H., Rheinhardt, M., & Käpylä, P. J. 2008b, ApJ, 676, 740

Brandenburg, A., Rädler, K.-H., Rheinhardt, M., & Subramanian, K. 2008c, ApJ, 687, L49

Brandenburg, A., Svedin, A., & Vasil, G. M. 2009, MNRAS, 395, 1599

Brandenburg, A., Schober, J., & Rogachevskii, I. 2017, Astron. Nachr., 338, 790

Chatterjee, P., Nandy, D., & Choudhuri, A. R. 2004, A&A, 427, 1019

Elperin, T., Kleeorin, N., & Rogachevskii, I. 2003, Phys. Rev. E, 68, 016311

Elperin, T., Golubev, I., Kleeorin, N., & Rogachevskii, I. 2007, Phys. Rev. E, 76, 066310

Elstner, D., & Rüdiger, G. 2000, A&A, 358, 612

Fournier, J.-D., Sulem, P.-L., & Pouquet, A. 1982, J. Phys. A Math. Gener., 15, 1393

Frank, J., King, A., & Raine, D. J. 2002, Accretion Power in Astrophysics: Third Edition (Cambridge, UK: Cambridge University Press)

Frisch, U., She, Z. S., & Sulem, P. L. 1987, Phys. D Nonlinear Phenom., 28, 382

Higham, D. J. 2001, SIAM Rev., 43, 525

Jurčišinová, E., Jurčišin, M., & Remecký, R. 2011, Phys. Rev. E, 84, 046311

Käpylä, P. J. 2019a, A&A, 622, A195

Käpylä, P. J. 2019b, Astron. Nachr., 340, 744

Käpylä, P. J., & Brandenburg, A. 2008, A&A, 488, 9

Käpylä, P. J., & Brandenburg, A. 2009, ApJ, 699, 1059

Käpylä, P. J., Korpi, M. J., & Brandenburg, A. 2009a, A&A, 500, 633

Käpylä, P. J., Mitra, D., & Brandenburg, A. 2009b, Phys. Rev. E, 79, 016302

Käpylä, P. J., Brandenburg, A., Korpi, M. J., Snellman, J. E., & Narayan, R. 2010, ApJ, 719, 67

Käpylä, M. J., Gent, F. A., Väisälä, M. S., & Sarson, G. R. 2018, A&A, 611, A15

Karak, B. B., Rheinhardt, M., Brandenburg, A., Käpylä, P. J., & Käpylä, M. J. 2014, ApJ, 795, 16

Karak, B. B., Miesch, M., & Bekki, Y. 2018, Phys. Fluids, 30, 046602

Kitchatinov, L. L., & Rüdiger, G. 2005, Astron. Nachr., 326, 379

Kitchatinov, L. L., Pipin, V. V., & Rüdiger, G. 1994, Astron. Nachr., 315, 157

Kleeorin, N., & Rogachevskii, I. 1994, Phys. Rev. E, 50, 2716

Krause, F., & Rädler, K.-H. 1980, Mean-field Magnetohydrodynamics and Dynamo Theory (Oxford: Pergamon Press)

Krause, F., & Rüdiger, G. 1974, Astron. Nachr., 295, 93

Krause, F., & Rüdiger, G. 1975, Sol. Phys., 42, 107

Madarassy, E. J. M., & Brandenburg, A. 2010, Phys. Rev. E, 82, 016304

Mitra, D., Käpylä, P. J., Tavakol, R., & Brandenburg, A. 2009, A&A, 495, 1

Moffatt, H. K. 1978, Magnetic Field Generation in Electrically Conducting Fluids (Cambridge: Cambridge University Press)

Petrovay, K., & van Driel-Gesztelyi, L. 1997, Sol. Phys., 176, 249

Rogachevskii, I., & Kleeorin, N. 2006, Geophys. Astrophys. Fluid Dyn., 100, 243

Rogachevskii, I., Kleeorin, N., & Brandenburg, A. 2018, J. Plasma Phys., 84, 735840502

Rüdiger, G. 1980, Geophys. Astrophys. Fluid Dyn., 16, 239

Rüdiger, G. 1982, Z. Angew. Math. Mech., 62, 95

Rüdiger, G. 1989, Differential Rotation and Stellar Convection. Sun and Solar-type Stars (Berlin: Akademie Verlag)

Rüdiger, G., & Kitchatinov, L. L. 2000, Astron. Nachr., 321, 75

Rüdiger, G., & Shalybkov, D. A. 2002, A&A, 393, L81

Rüdiger, G., Kitchatinov, L. L., & Brandenburg, A. 2011, Sol. Phys., 269, 3

Rüdiger, G., Kitchatinov, L. L., & Hollerbach, R. 2013, Magnetic Processes in Astrophysics: Theory, Simulations, Experiments (Weinheim: Wiley-VCH)

Schrinner, M., Rädler, K.-H., Schmitt, D., Rheinhardt, M., & Christensen, U. 2005, Astron. Nachr., 326, 245

Schrinner, M., Rädler, K.-H., Schmitt, D., Rheinhardt, M., & Christensen, U. R. 2007, Geophys. Astrophys. Fluid Dyn., 101, 81

Shakura, N. I., & Sunyaev, R. A. 1973, A&A, 24, 337

Snellman, J. E., Käpylä, P. J., Korpi, M. J., & Liljeström, A. J. 2009, A&A, 505, 955

Sur, S., Brandenburg, A., & Subramanian, K. 2008, MNRAS, 385, L15

Väisälä, M. S., Brandenburg, A., Mitra, D., Käpylä, P. J., & Mantere, M. J. 2014, A&A, 567, A139

Verma, M. K. 2001, Phys. Plasma, 8, 3945

Yokoi, N. 2018, J. Plasma Phys., 84, 735840501

Yokoi, N., & Brandenburg, A. 2016, Phys. Rev. E, 93, 033125

Yousef, T. A., Brandenburg, A., & Rüdiger, G. 2003, A&A, 411, 321

Appendix A: Justification for Eq. (15)

In the isothermal case, it is convenient to consider the quantity $H = \ln \rho$ instead of the density itself resulting in equations linear in $\overline{H}$ and free of triple correlations of fluctuating quantities. We denote the turbulence present under the condition $\overline{U} = \nabla \overline{H} = \mathbf{0}$ by $\boldsymbol{u}^{(0)}$. If $\boldsymbol{u}^{(0)}$ describes isotropic turbulence, only the diagonal components Q_{ii} exist. Proceeding to the situation $\overline{U} = \mathbf{0}, \nabla \overline{H} \neq \mathbf{0}$, indicated by the superscript $(0, \overline{H})$ the fluctuations $\boldsymbol{u}, h$ can be written as $\boldsymbol{u} = \boldsymbol{u}^{(0)} + \boldsymbol{u}^{(0,\overline{H})}$, $h = h^{(0)} + h^{(0,\overline{H})}$. Correspondingly, the mean force is

$$\mathcal{F} = 2\nu \overline{\mathbf{s} \cdot \nabla h} - \overline{\boldsymbol{u} \cdot \nabla \boldsymbol{u}} = \mathcal{F}^{(0)} + \mathcal{F}^{(0,\overline{H})} \tag{A.1}$$

with $\mathbf{s} = \mathbf{S} - \overline{\mathbf{S}}$, and

$$\mathcal{F}^{(0)} = 2\nu \overline{\mathbf{s}^{(0)} \cdot \nabla h^{(0)}} - \overline{\boldsymbol{u}^{(0)} \cdot \nabla \boldsymbol{u}^{(0)}}, \tag{A.2}$$

$$\mathcal{F}^{(0,\overline{H})} = 2\nu \left(\overline{(\mathbf{s}^{(0)} + \mathbf{s}^{(0,\overline{H})}) \cdot \nabla h^{(0,\overline{H})} + \mathbf{s}^{(0,\overline{H})} \cdot \nabla h^{(0)}} \right)$$
$$- \overline{(\boldsymbol{u}^{(0)} + \boldsymbol{u}^{(0,\overline{H})}) \cdot \nabla \boldsymbol{u}^{(0,\overline{H})}} - \overline{\boldsymbol{u}^{(0,\overline{H})} \cdot \nabla \boldsymbol{u}^{(0)}}. \tag{A.3}$$

Restricting to first order in the mean quantities, we get

$$\mathcal{F}^{(0,\overline{H})} = 2\nu \left(\overline{\mathbf{s}^{(0)} \cdot \nabla h^{(0,\overline{H})} + \mathbf{s}^{(0,\overline{H})} \cdot \nabla h^{(0)}} \right)$$
$$- \overline{\boldsymbol{u}^{(0)} \cdot \nabla \boldsymbol{u}^{(0,\overline{H})}} - \overline{\boldsymbol{u}^{(0,\overline{H})} \cdot \nabla \boldsymbol{u}^{(0)}}. \tag{A.4}$$

Analogously, for $\overline{U} \neq \mathbf{0}, \nabla \overline{H} = \mathbf{0}$, we have

$$\mathcal{F} = \mathcal{F}^{(0)} + \mathcal{F}^{(\overline{U},0)} \tag{A.5}$$

with

$$\mathcal{F}^{(\overline{U},0)} = 2\nu \left(\overline{\mathbf{s}^{(0)} \cdot \nabla h^{(\overline{U},0)} + \mathbf{s}^{(\overline{U},0)} \cdot \nabla h^{(0)}} \right)$$
$$- \overline{\boldsymbol{u}^{(0)} \cdot \nabla \boldsymbol{u}^{(\overline{U},0)}} - \overline{\boldsymbol{u}^{(\overline{U},0)} \cdot \nabla \boldsymbol{u}^{(0)}} \tag{A.6}$$

in first order. If now both $\overline{U}$ and $\nabla \overline{H}$ do not vanish, one can see from the equations for the fluctuating quantities, again restricted to first order in the mean quantities,

$$\partial_t h^{(\overline{U},\overline{H})} = -\overline{U} \cdot \nabla h^{(0)} - \boldsymbol{u}^{(0)} \cdot \nabla \overline{H} - \nabla \cdot \boldsymbol{u}^{(\overline{U},\overline{H})} \tag{A.7}$$
$$- \left(\boldsymbol{u}^{(0)} \cdot \nabla h^{(\overline{U},\overline{H})} + \boldsymbol{u}^{(\overline{U},\overline{H})} \cdot \nabla h^{(0)} \right)',$$

$$\partial_t \boldsymbol{u}^{(\overline{U},\overline{H})} = -c_s^2 \nabla h^{(\overline{U},\overline{H})} + \nu \nabla^2 \boldsymbol{u}^{(\overline{U},\overline{H})} \tag{A.8}$$
$$+ 2\nu \left(\mathbf{s}^{(0)} \cdot \nabla h^{(\overline{U},\overline{H})} + \mathbf{s}^{(\overline{U},\overline{H})} \cdot \nabla h^{(0)} \right)'$$
$$- \left(\boldsymbol{u}^{(0)} \cdot \nabla \boldsymbol{u}^{(\overline{U},\overline{H})} + \boldsymbol{u}^{(\overline{U},\overline{H})} \cdot \nabla \boldsymbol{u}^{(0)} \right)'$$
$$+ 2\nu \left(\mathbf{s}^{(0)} \cdot \nabla \overline{H} + \overline{\mathbf{S}} \cdot \nabla h^{(0)} \right) \tag{A.9}$$
$$- \boldsymbol{u}^{(0)} \cdot \nabla \overline{U} - \overline{U} \cdot \nabla \boldsymbol{u}^{(0)},$$

that due to their linearity in $h^{(\overline{U},\overline{H})}$, $\boldsymbol{u}^{(\overline{U},\overline{H})}$, and the additivity of their inhomogeneities depending on $\overline{U}$ and $\overline{H}$, respectively,

$$h^{(\overline{U},\overline{H})} = h^{(0,\overline{H})} + h^{(\overline{U},0)}, \tag{A.10}$$

$$\boldsymbol{u}^{(\overline{U},\overline{H})} = \boldsymbol{u}^{(0,\overline{H})} + \boldsymbol{u}^{(\overline{U},0)}, \tag{A.11}$$

holds and hence

$$\mathcal{F} = \mathcal{F}^{(0)} + \mathcal{F}^{(\overline{U},0)} + \mathcal{F}^{(0,\overline{H})} \tag{A.12}$$

to first order in $\overline{U}$ and $\overline{H}$. Given that the major part of $\mathcal{F}$ is $\nabla \cdot \boldsymbol{Q}$, an equivalent relationship can be assumed for $\boldsymbol{Q}$.